

Supporting Information for

**Increased charge transfer state separation  
via reduced mixed phase interface in polymer solar cells**

Thomas Ferron, Matthew Waldrip, Michael Pope, Brian A. Collins\*  
Department of Physics and Astronomy, Washington State University, Pullman, WA 99164

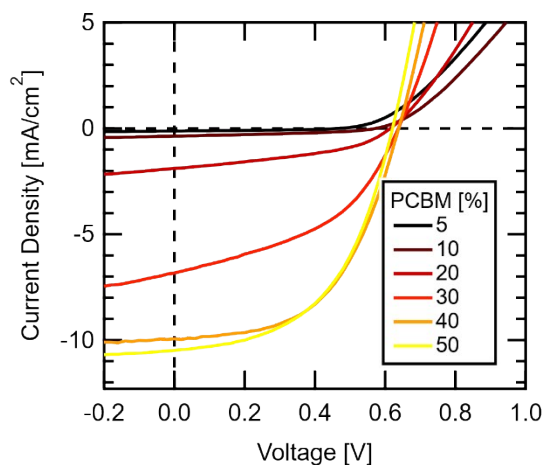


Figure S1: Linear scale JV curve of all device blends given in Figure 1a of the main text.

Blend Ratio [PCBM wt.%]	$J_{sc}$ (mA/cm <sup>2</sup> )	$V_{oc}$ (V)	FF (%)	PCE (%)
5	0.13 (2)	0.48 (1)	40.3 (1)	0.030 (5)
10	0.40 (2)	0.580 (1)	40.0 (1)	0.09 (1)
20	1.95 (4)	0.61 (1)	41.5 (1)	0.49 (1)
30	6.6 (5)	0.640 (1)	42 (1)	1.8 (2)
40	9.9 (3)	0.64 (1)	52 (1)	3.2 (1)
50	10.1 (2)	0.62 (1)	52 (1)	3.23 (7)

Table S1: JV device metrics given in Figure 1b / 1c from the main text.

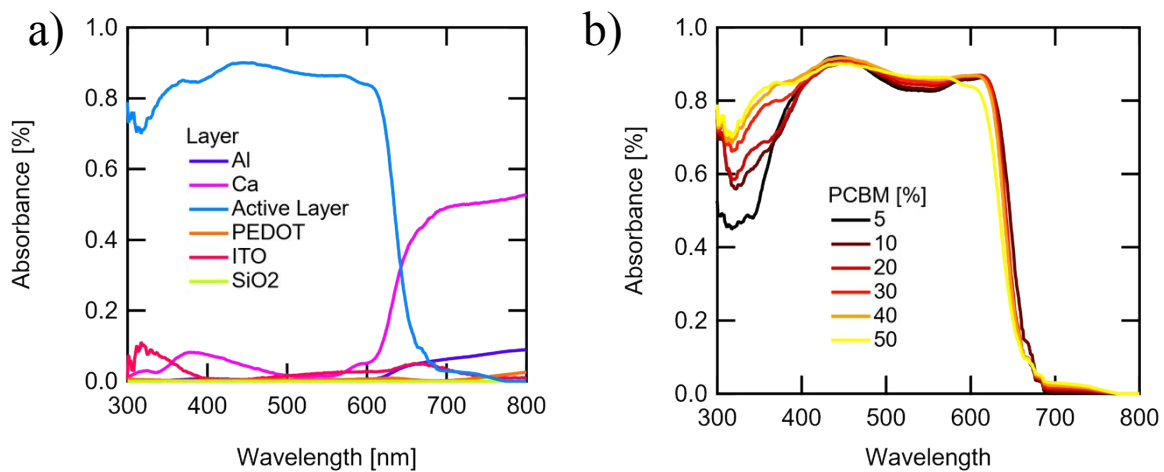


Figure S2: (a) Transfer matrix modeling for optical absorbance of 50 wt. PCBM device including all component layers. Software used for calculation was developed by the McGehee group (see main text reference). Simulated device stack mirrors device fabrication ITO(110nm):PEDOT(10nm):Active Layer(XXX):Ca(25nm):Al(150nm). Active layer thickness was measured with transmission NEXAFS at the location of scattering (Figure S11). (b) Active layer absorbance for all device blends investigated in study.

### Photoluminescence Quenching:

PLQ is calculated as the ratio between integrated PL intensities from each blend device and reference films. Calculating total reference PL is done by scaling each component PL to the mass concentration of each material

$$PLQ(x) = \frac{\int PL_x(\lambda) d\lambda}{(1-x)\int PL_{p3HT}(\lambda) d\lambda + x\int PL_{PCBM}(\lambda) d\lambda}$$

where  $x$  is the wt.% PCBM in the blend film and  $PL_x(\lambda)$  is the measured PL for a device with associated PCBM wt.%.

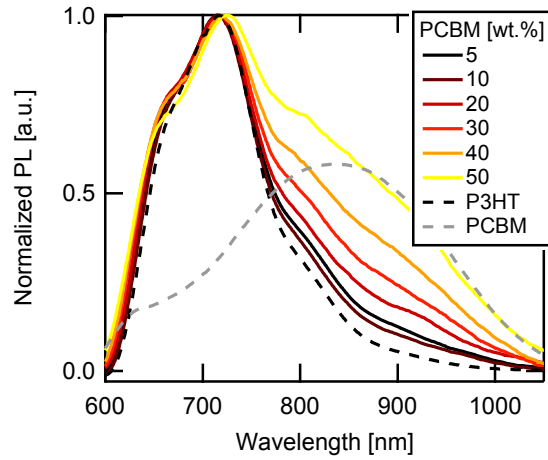


Figure S3: Normalized PL for all blends and reference films. PCBM PL in the blends begin to show up at 20 wt.% PCBM.

## Calculating Generation Current

Generation current  $J_G(V)$  is a measure of the possible current available assuming all charges are extracted following CT State separation. We calculate this value by scaling the total charge extracted from integrated TDCF transients to the measured photocurrent measured at -3V bias. Figure S4 gives the total charge extracted against the measured photocurrent for every device. To ensure an equal scaling between devices the fitted slope gives a conversion between charge extracted and photocurrent allowing a direct comparison between generated charge as a current density as shown in Figure 2c of the main text.

Resulting fit is given by  $Q_{tot}(J_{ph}) = -0.6 \cdot J_{ph} + 0.25$  where  $Q_{tot}$  is the total charge extracted from TDCF and  $J_{ph} = J_{light} - J_{dark}$  is the measured photocurrent.

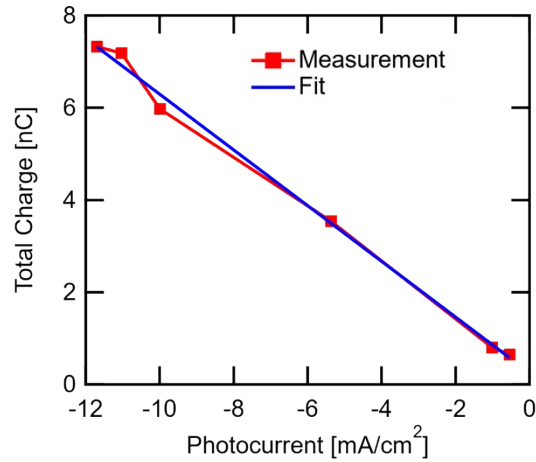


Figure S4: Charge extracted plotted against photocurrent for each measured device. Linear fit gives conversion for total charge and generation current as discussed in the main text.

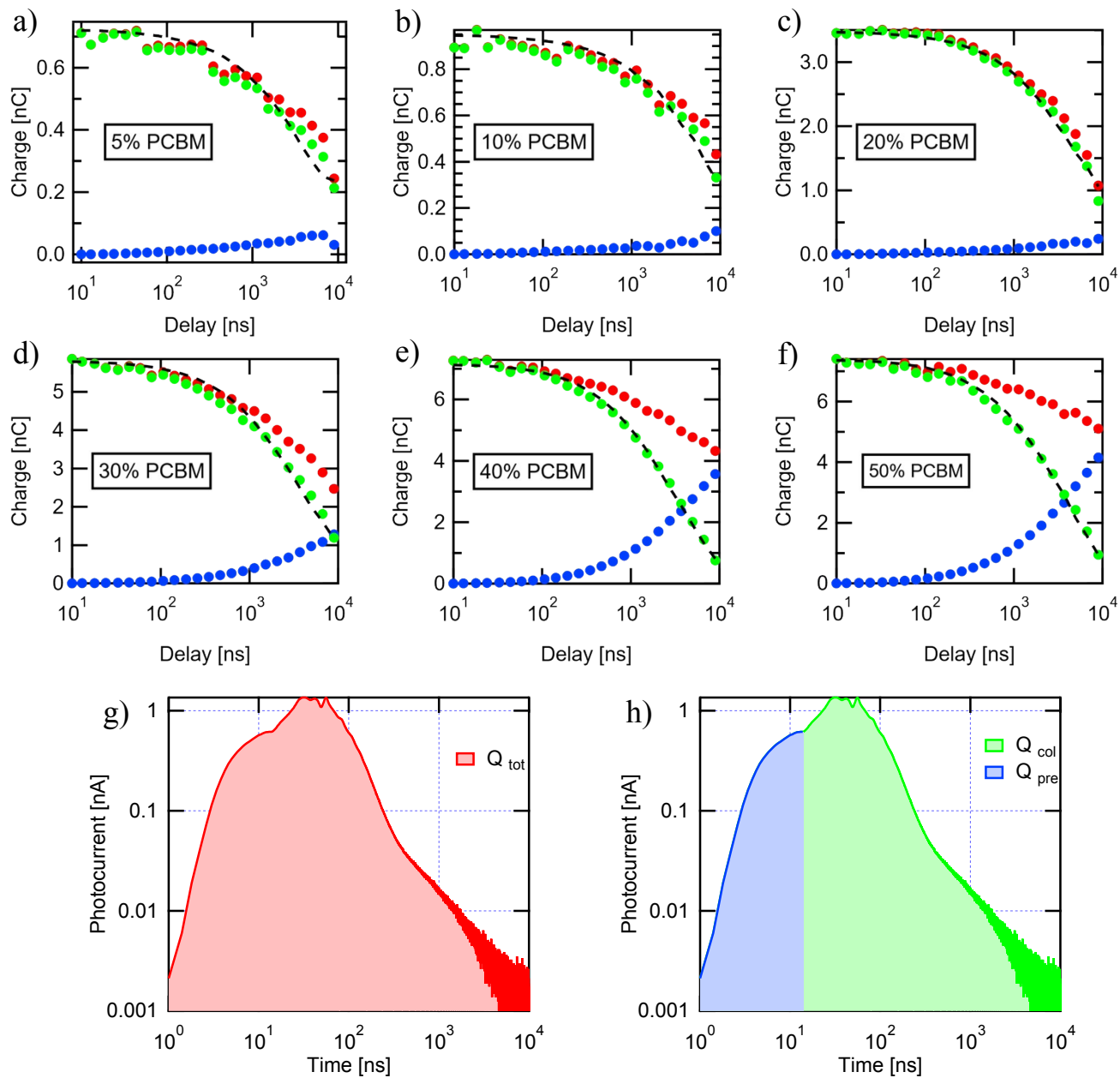


Figure S5: Summary graphs for delay dependent TDCF. (a-f) Individual measurements of  $Q_{pre}$  (blue)  $Q_{tot}$  (red), and  $Q_{col}$  (green) for each device. Fits to the collected charge following second order rate equation (as discussed in the text) is given in black. (g-h) Schematic of TDCF transient data processing. Total integrated photocurrent transient gives  $Q_{tot}$ , the area following laser excitation before extraction pulse gives  $Q_{pre}$ , and the charge collected after excitation gives  $Q_{col}$ . The example shown is for  $t_d = 10$  ns.

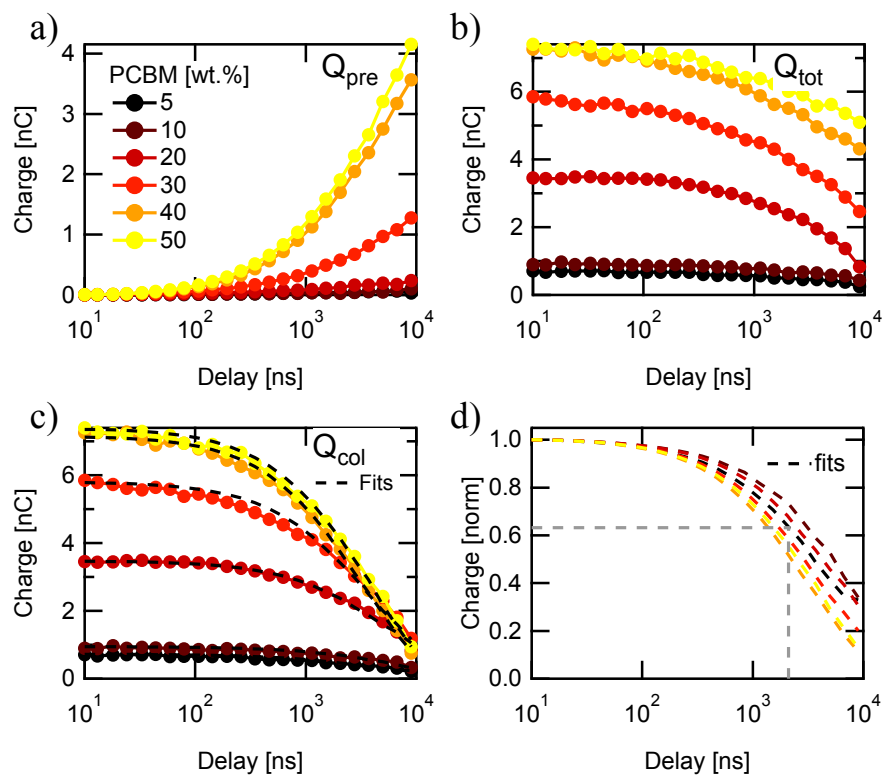


Figure S6: (a-c) Comparison graphs for  $Q_{pre}$ ,  $Q_{tot}$ , and  $Q_{col}$  from Figure S5. Legend colors apply to all sub-graphs (b-d). (d) Normalized  $Q_{col}$  fits. Charge lifetime  $\tau = (1 - e^{-1})$  from extraction  $\approx 2 \mu s$ . Indicated by grey dashed line.

## Maximum current calculation

To solve for the maximum current available to a given OPV, we assume they operate with 100% quantum efficiency. To calculate the total number of photons from our AAA solar simulator we measure the spectra (Grey area in Figure S7 displayed as photon irradiance) with an Ocean Optics QEpro spectrometer and scale the power to  $1000W/m^2$ . The total number of absorbed photons (up to a cutoff wavelength  $\lambda_{max}$ ) is then calculated by integrating the photon irradiance  $I_{ph}(\lambda)$ . Multiplying by the charge of an electron gives  $J_{max}$  as discussed in the text.

$$J_{max} = e \int_{300}^{\lambda_{max}} I_{ph}(\lambda) d\lambda$$

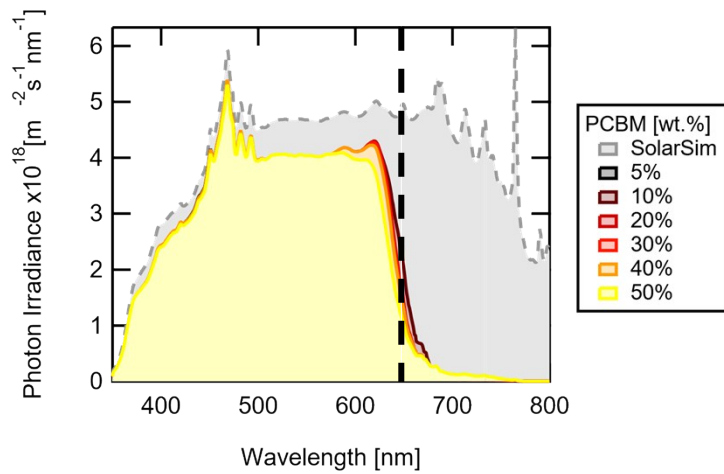


Figure S7: Photon irradiance of our AAA solar simulator (grey). Color scale highlights the solar simulator scaled to the calculated absorbance of each device from Figure S2(b). Dotted black line is a guide to the eye for the cutoff wavelength of 650nm.

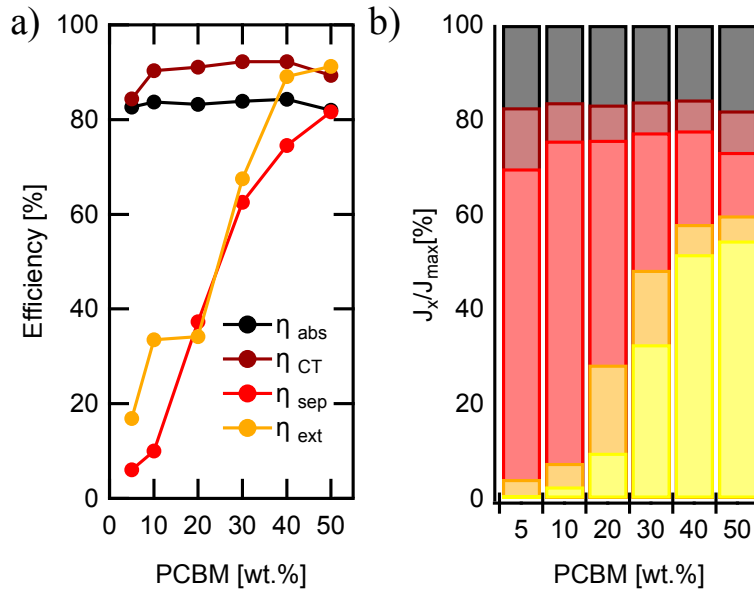


Figure S8: (a) Efficiency of each charge generation process as a function of PCBM wt.% at short circuit conditions. (b) Composite figure of charge density at each step in the process. From top to bottom, each colored region represents excited state populations relative to  $J_{max}$ : Photons not absorbed by the active layer (black), exciton recombination (maroon), geminate recombination (red), bimolecular recombination (orange), and charge extracted (yellow).

Blend Ratio [PCBM wt.%]	Photons not absorbed [%]	Exciton Recomb. [%]	Geminate Recomb. [%]	Bimolecular Recomb. [%]	Charge Extracted [%]
5	17.4	9.0	69.4 (69.2)	3.5 (3.9)	0.7 (0.5)
10	16.3	4.7	71.5 (72.3)	5.0 (5.2)	2.5 (1.5)
20	16.8	4.6	50.2 (50.9)	18.6 (22.7)	9.8 (5.0)
30	16.1	3.9	31.6 (33.3)	15.7 (27.7)	32.7 (19.0)
40	15.7	3.8	22.6 (23.3)	6.3 (17.3)	51.6 (39.9)
50	18	5.5	16.7 (15.8)	5.2 (19.3)	54.6 (41.4)

Table S2: Relative charge losses at each point in charge generation process compared to incident flux. Represented as colored areas in Figure 3b (MPP in red) and Figure S8b ( $J_{sc}$  in black). First two steps are voltage independent.

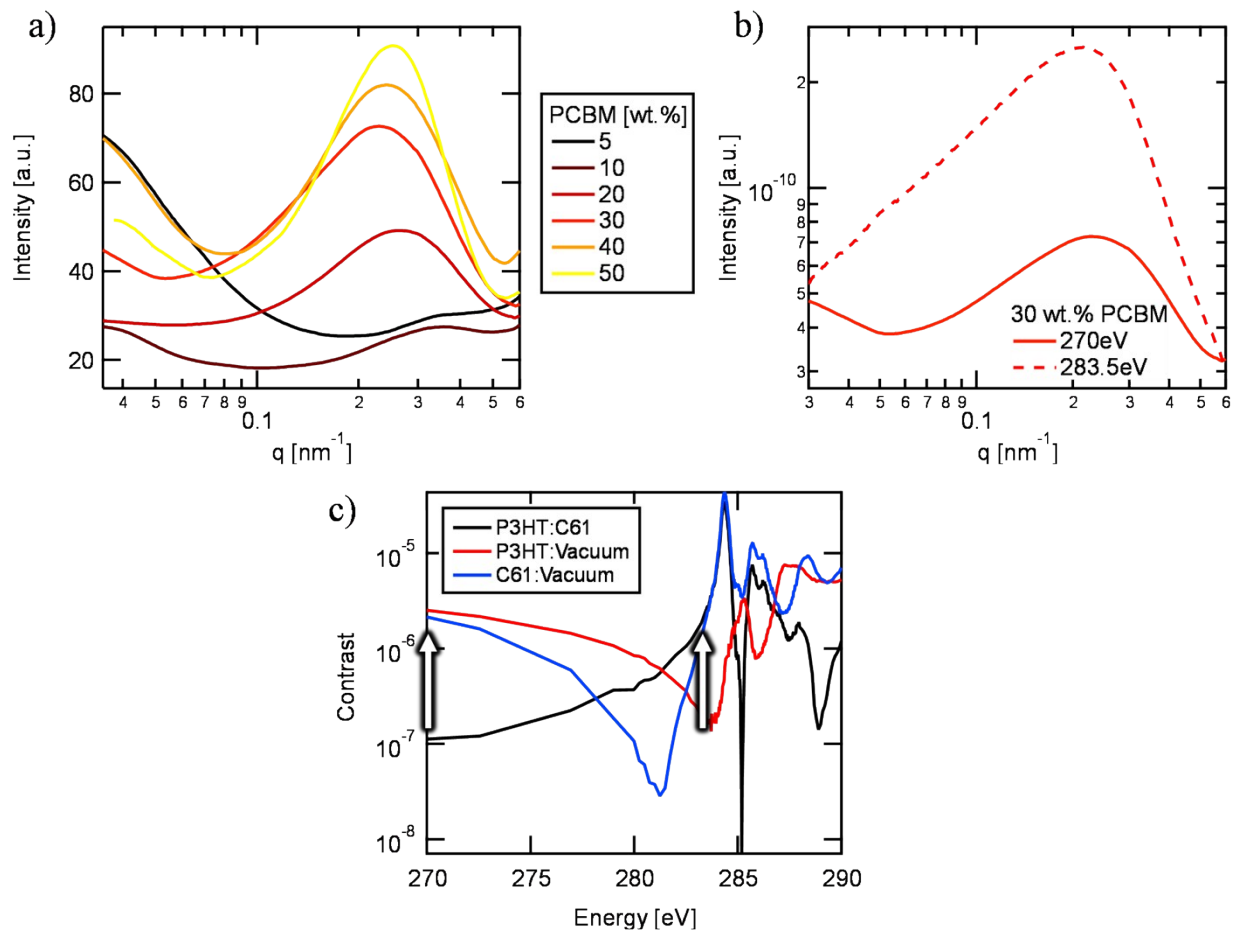
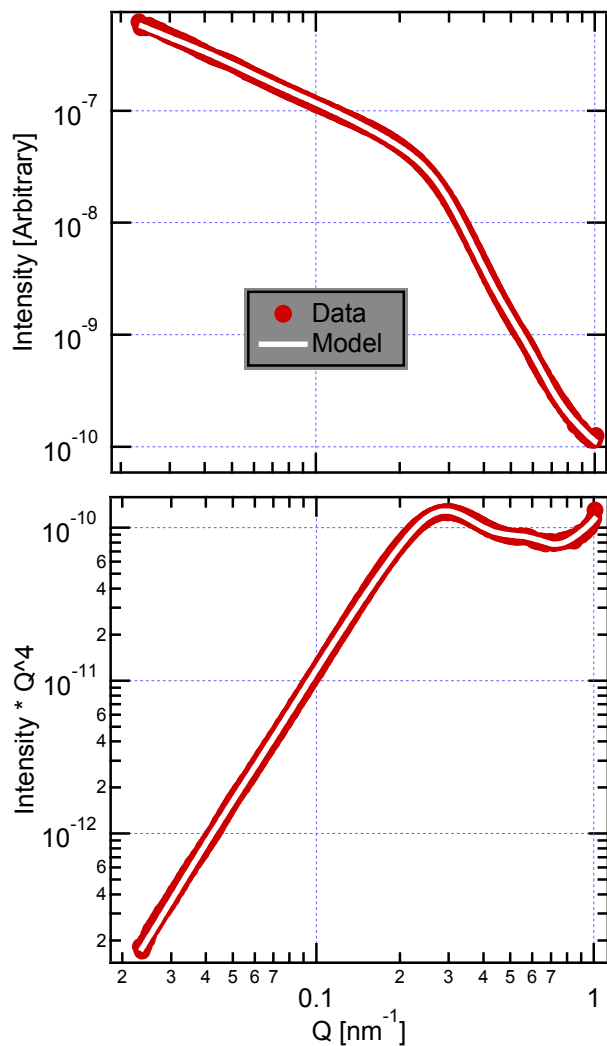


Figure S9: (a) RSoXS taken at 270eV (off-resonant). Upward sloped feature at  $q < 0.1 \text{ nm}^{-1}$  is seen for all devices and has a higher relative intensity to the primary peak at  $q = 0.23 \text{ nm}^{-1}$  compared to 283.5eV. This energy dependence tracks the material contrast function  $C = \Delta\delta^2 + \Delta\beta^2$  as we expect higher scattering from vacuum (roughness) interactions at 270eV. (b) Example comparison between near and off-resonant scattering for 30 wt.% PCBM. (c) Contrast functions between P3HT:PCBM and each component with vacuum. Arrows indicate energies where reported scattering occurs.



	Parameter	Value
Cylinder Form Factor	Mean Radius	9.0 nm
	FWHM	9 nm
	Aspect Ratio	1200
Hard Sphere	Spacing	21 nm
	Vol Fraction	15%

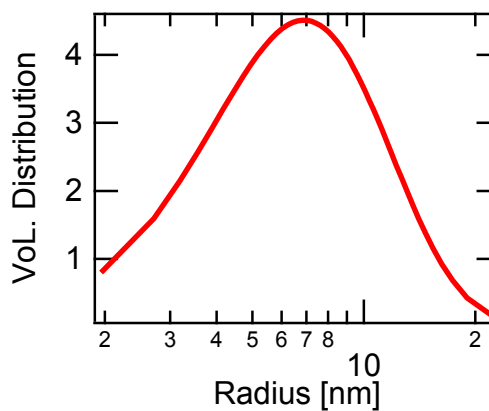


Figure S10: Particle scattering fit to the 30 wt.% PCBM blend film RSoXS profile at 283.5 eV (other films are similar). Data and model are displayed in two different formats in the panels on the left for better inspection. Analysis done in the IRENA package by Jan Ilavsky. A cylinder form factor (3 parameters) with a hard sphere structure factor (two parameters) is used with the parameters and fit values shown in the top right table. The volume distribution of cylinder radii is displayed in the lower right panel. Notably, the model is similar without the structure factor but improves the fit by flattening the scattering profile at  $Q < 0.2 \text{ nm}^{-1}$ . This supports the view that the scattering features originate primarily from the fibril size rather than a spacing.

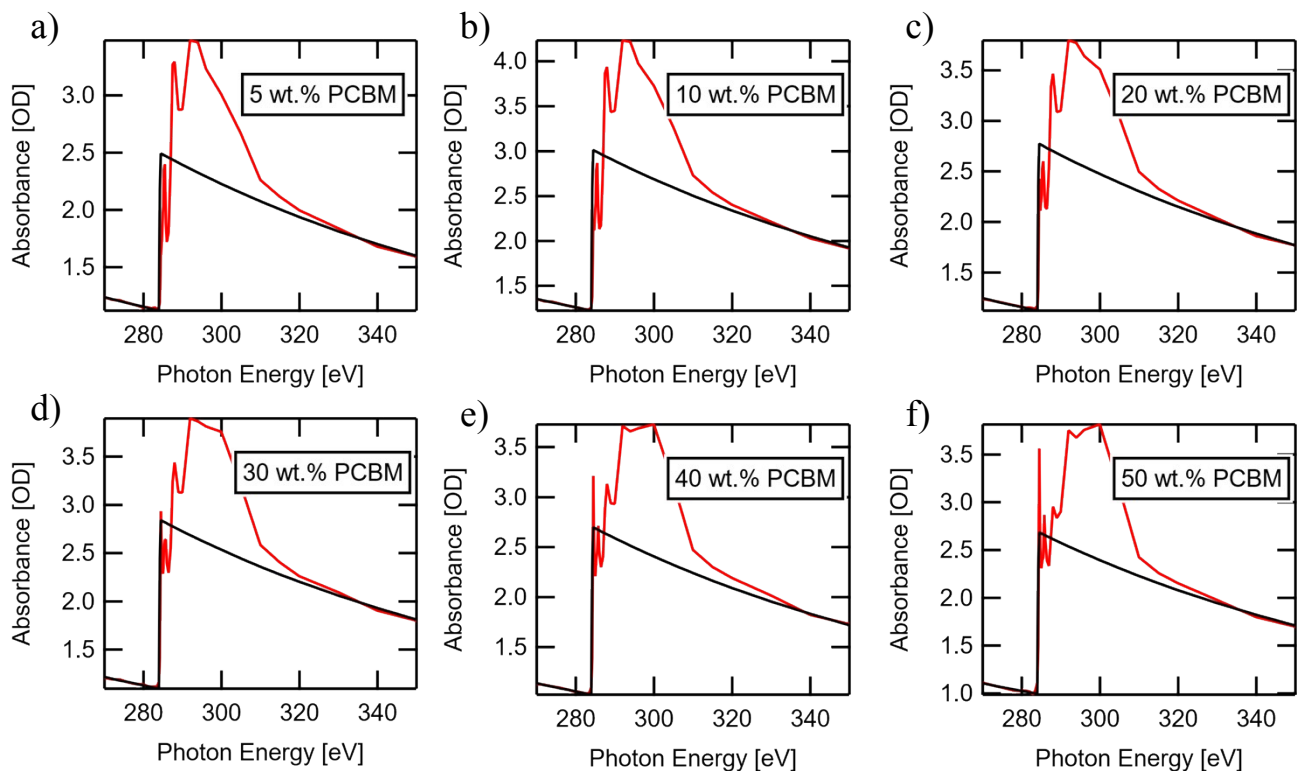


Figure S11: (a-f) NEXAFS spectra (red) fit to the bare atom mass absorption (black) of each device blend. Thickness is extracted using Beer-Lambert law  $\ln(I(E)/I_0(E)) = \mu(E)\rho t$ , where  $\ln(I(E)/I_0(E))$  is the ratio of intensity measured through device and the reference beam giving the optical density  $OD$  as displayed in the figure,  $\mu(E)$  is the mass absorption,  $\rho$  is the mass density, and  $t$  is the thickness. Using the known mass absorption before and after the absorption edge from the Center for X-ray Optics database one can calculate the thickness. NEXAFS measurement is taken at location of scattering to extract thickness of film at scattering position.

Blend Ratio [wt.% PCBM]	Thickness [nm]
5	299(3)
10	372(2)
20	325(2)
30	332(3)
40	312(1)
50	310(3)

Table S3: Thickness parameters extracted from bare atom fits to NEXAFS spectra.

### GIWAXS Analysis:

Peak identification was done through comparison to pure films of blend components. Figure S12 gives the circular averaged profiles of both P3HT and PCBM at an incident angle of  $0.2^\circ$ . P3HT exhibits its characteristic (100) diffraction peak at  $q = 3.9\text{nm}^{-1}$  corresponding to lamellar packing of  $d = 1.6\text{nm}$  (P3HT (200) and (300) reflections are also present at  $q \approx 7.7\text{nm}^{-1}$  and  $q \approx 11.6\text{nm}^{-1}$  respectively). A small feature is found at  $q = 13.5\text{nm}^{-1}$  that we attribute to amorphous P3HT as this feature is isotropic. Additionally, the  $\pi - \pi$  stacking at  $q = 16.5\text{nm}^{-1}$  exists for all measured samples demonstrating all films contain aggregate P3HT forming fibril structures.

PCBM has a broad shoulder ranging from  $\approx 5.8\text{nm}^{-1}$  which overlaps with the (100) and (200) P3HT reflections making it difficult to quantify in the blend films. Instead, for our analysis we focus at the peak centered at  $q \approx 13.9\text{nm}^{-1}$  that only overlaps a weakly diffracting amorphous P3HT feature.

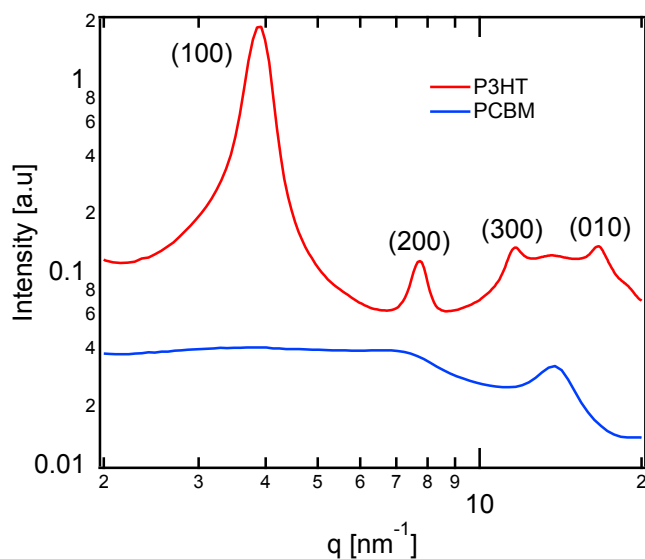


Figure S12: Circular averaged profiles of component GIWAXS. Data taken at  $0.2^\circ$ .

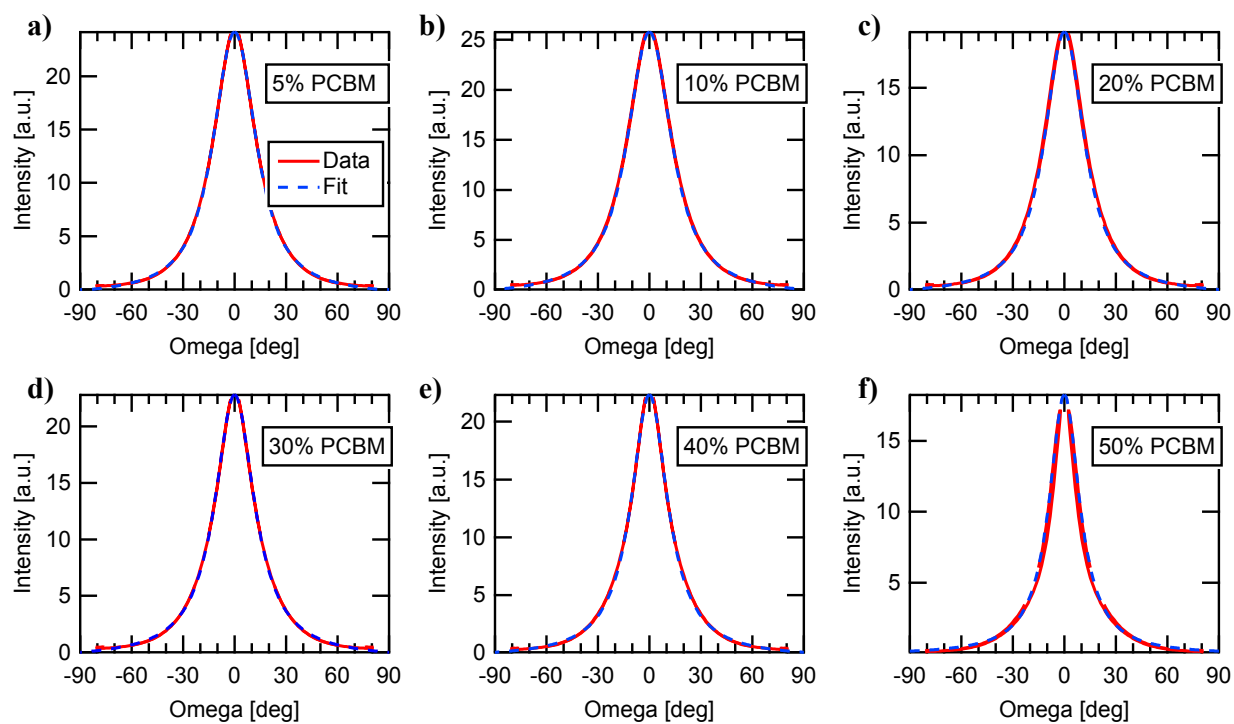


Figure S13: Pole Figures of P3HT (100) extracted from GIWAXS intensities. Legend colors apply to all sub-graphs (b-f). A linear background was subtracted from the integrated intensities across the diffraction peak at each azimuthal angle which is converted to reciprocal space polar angle. Resultant pole figures are fit to a Voigt function (pictured) to account for scattering not directly captured at detector edges  $\omega \approx 90^\circ$  or specular condition  $\omega \approx 0^\circ$ . Relative degree of crystallinity is calculated through

$$rDOC = \int_0^{90^\circ} I_{PF}(\omega) \sin(\omega) d\omega$$

integrating the pole figure  $I_{PF}(\omega)$ ,



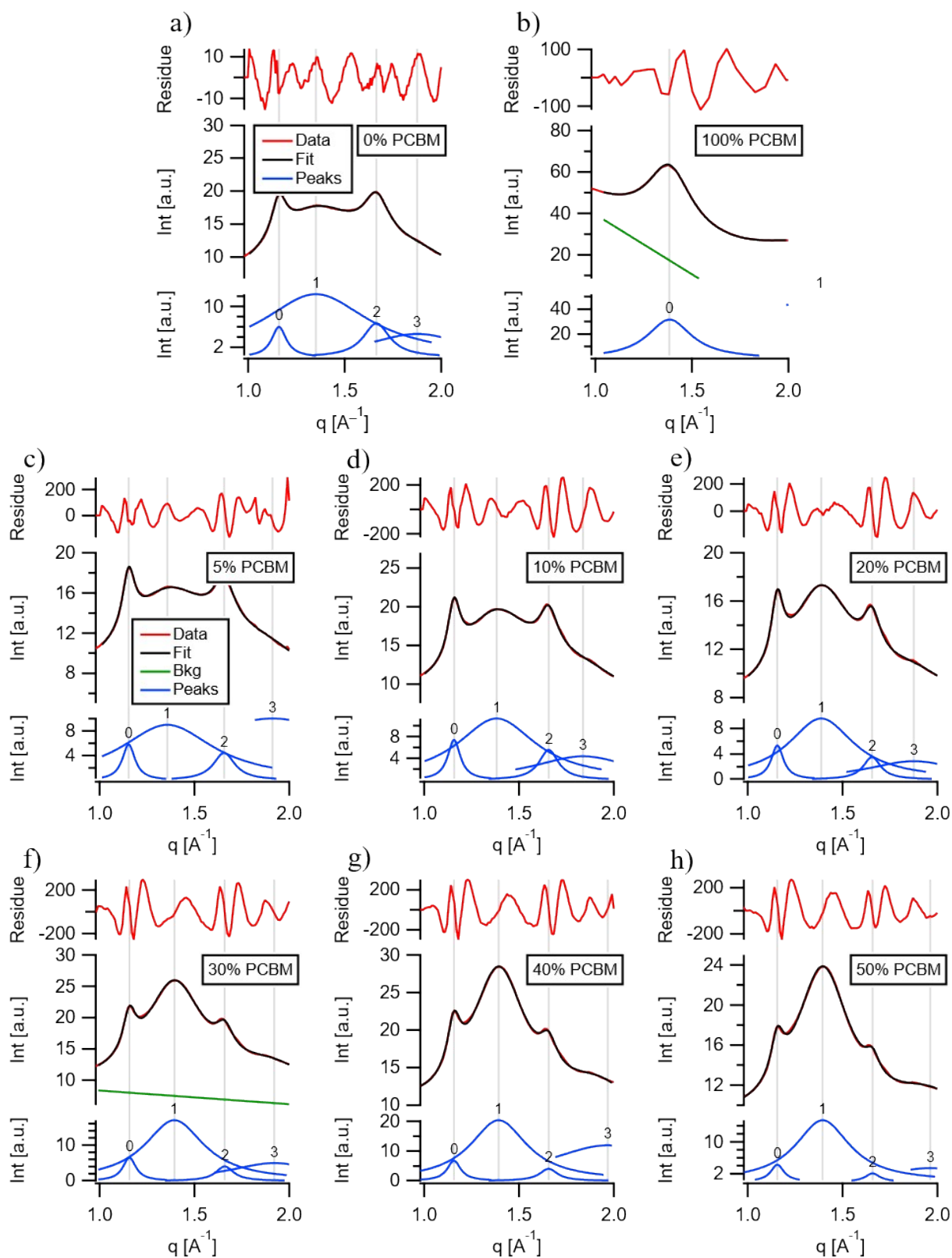


Figure S14: GIWAXS component fitting to PCBM peak. Circularly averaged scattering intensity profiles were fit to four Lorentzians for each visible feature with a linear background in the region shown. (a) Pure P3HT film (b) Pure PCBM film (c-h) Device blends from the study. Legend colors apply to all sub-graphs.

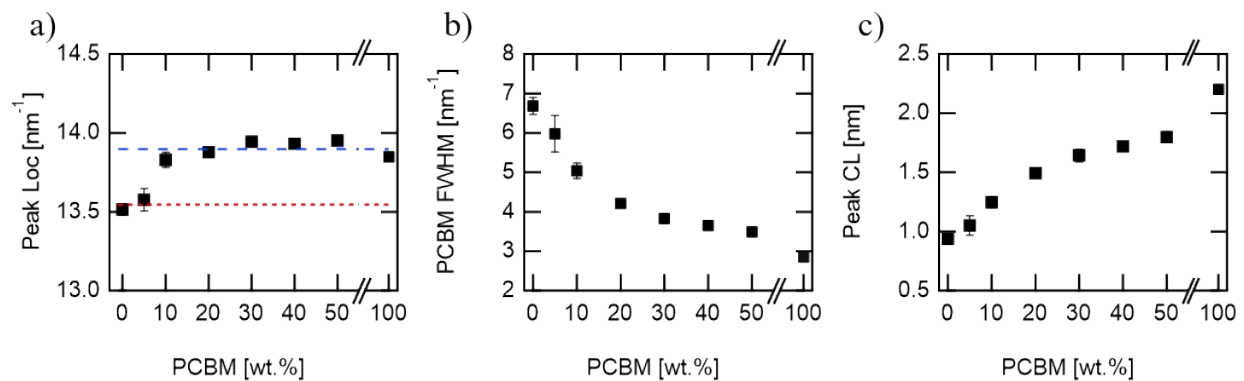


Figure S15: Peak fit results from peak 1 in SI Figure 14. (a) Peak location, horizontal red line shows location of amorphous P3HT halo while blue line shows the approximate position of the PCBM feature. (b) Peak 1 Full width half max as a function of PCBM wt.%. (c) Peak 1 correlation length as a function of PCBM wt.%. Correlation length is calculated from the Scherrer equation  $CL = 2\pi/FWHM$ .

**Resonant Scattering Model:** Modeling the total scattering intensity over  $N$  total domains can be represented as a sum over volume fraction products scaled by relative scattering contrast,

$$TSI(E) = 2\pi^2 \sum_{i \neq j}^N |\Delta\rho_{ij}(E)|^2 \phi_i \phi_j \#(1)$$

where  $TSI(E)$  is the total scattering intensity,  $\Delta\rho_{ij}(E)$  is the difference in scattering length density between domains  $i$  and  $j$ , and  $\phi_i$  is the volume fraction of domain  $i$ . Contrast from the scattering length density can be converted to the complex index of refraction through the following relationship,

$$|\Delta\rho_{ij}(E)|^2 = \frac{2\pi^2}{(hc)^4} E^4 |\Delta n_{ij}|^2 \#(2)$$

where  $h$  is Planks constant,  $c$  is the speed of light,  $E$  is the energy, and  $\Delta n_{ij}$  is the difference in complex index of refraction between domains  $i$  and  $j$  as discussed in the main text.

To extract domain composition, we can differentiate between the index of refraction of a domain to that of a pure material. We will approximate the index of refraction of a domain to be a weighted average between its  $m$  constitute components,

$$n = \sum_{k,i}^m x_{ki} n_k \#(3)$$

where  $n$  is the index of refraction for a single domain,  $n_k$  is the index of refraction of component  $k$ , and  $x_{ki}$  is the mass fraction of material  $k$  in domain  $i$ . Such that,

$$\sum_k x_{ki} = 1 \#(4)$$

For a two-component system comprised of a donor (molecule  $D$ ) and acceptor (molecule  $A$ ) the material contrast reduces to,

$$\Delta n_{ij} = \Delta n_{DA} \Delta x_{ij} \#(5)$$

Substituting into Equation (1) we are left with,

$$TSI(E) = \frac{4\pi^2}{(hc)^4} E^4 |\Delta n_{DA}(E)|^2 \sum_{i \neq j}^N |\Delta x_{ij}|^2 \phi_i \phi_j \#(6)$$

giving the relationship from the main text where  $\alpha = \frac{4\pi^2}{(hc)^4} E^4 |\Delta n_{DA}(E)|^2$ .

To quantify the phase volumes in terms of the total material mass within the system we can write the component blend ratio as,

$$R_m = \frac{M_D}{M_A} = \frac{\sum_{i=1}^N \phi_i \rho_i x_{Di}}{\sum_{j=1}^N \phi_j \rho_j x_{Aj}} \quad \#(7)$$

$R_m$  is the ratio of the component masses,  $M_k$  is the total mass of a component  $k$ ,  $\phi_i$  is the volume fraction of domain  $i$ ,  $\rho_i$  is the density of domain  $i$ . Rewriting equation 7 in terms of the P3HT mass balance it can track the total mass fraction of P3HT in the crystal phase.

$$f_{wt} = \frac{M_c}{M_a} = \frac{\phi_p \rho_p}{\phi_m \rho_m x_m} \quad \#(8)$$

where  $\frac{M_c}{M_a}$  is the ratio of P3HT mass (weight) between the crystal and amorphous phase, the subscript  $p$  references the P3HT crystal phase while the subscript  $m$  references the mixed phase as discussed in the main text. Putting equation (7) and (8) together for two or three phases we are left with our equation for the volume fractions

$$\phi_m(R_m) = \frac{R_m + (f_{wt} + 1)}{(f_{wt} + 1) + R_m \left(1 + \frac{\rho_m}{\rho_p} f_{wt}\right)} \quad \#(9)$$

$$\phi_m(R_m, x_m) = \frac{\rho_f}{\rho_m} \left[ \frac{x_m}{R_m} (f_{wt} + 1) - (1 - x_m) + \rho_f \left( \frac{1}{\rho_m} + \frac{x_m f_{wt}}{\rho_p} \right) \right]^{-1} \quad \#(10)$$

where equation (9) is solved for two-phases and (10) for three-phases.

All RSoXS TSI fitting was completed using IGOR Pros built-in least chi squared algorithm along with a custom fit function. Total unknowns in the system include: Volume fraction and composition of the mixed phase ( $\phi_m x_m$ ), a scale factor for RSoXS intensity, and the amount of orientation fluctuations from P3HT that will provide background signal in addition to material scattering.

Total scattering intensity is fit to both two and three domain models where a transition between the two occurs when the concentration of the mixed phase matches both models. The two-domain model consists of two fit parameters: RSoXS intensity scale factor and the additive background. Given a mass of crystallization, the composition of the mixed phase can be calculated based on the blend ratio and density of components. Upon increasing PCBM wt.% within the blend, the mixed phase will swell, and the composition will become more PCBM rich. The three-domain model consists of three fit parameters, the same intensity scale factor and background as the two-domain model in addition to the mixed phase composition. Here, we consider the mixed phase to be saturated and any additional PCBM will aggregate into a pure phase.

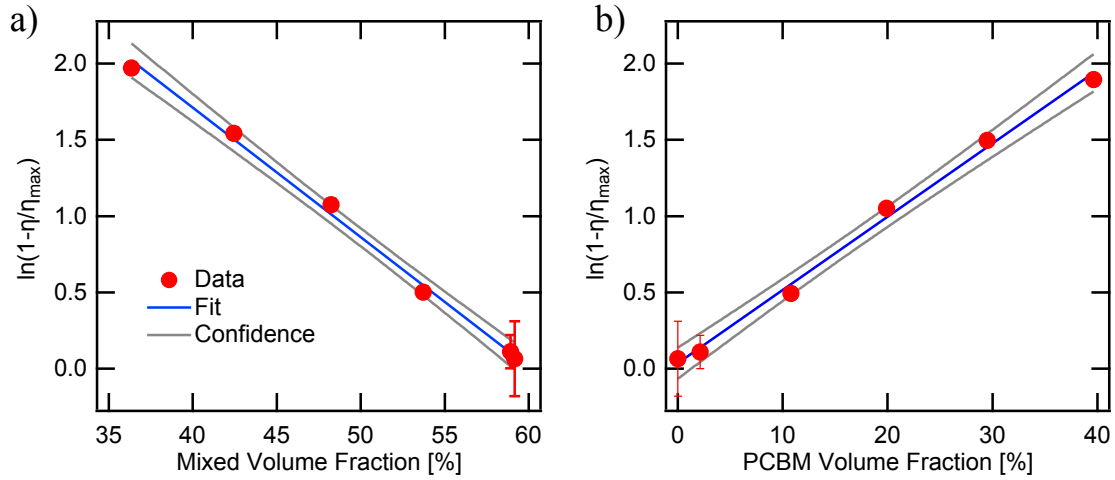


Figure S16: Linear plots of separation efficiency as a function of volume fraction. In order to remove exponential dependence, we convert the separation efficiency to  $\ln(1-\eta/\eta_{max})$  where  $\eta_{max}$  is the saturation efficiency as discussed in the main text. Displayed confidence intervals are 95% and  $R^2$  values are 0.996 and 0.995 for the mixed volume fit and the PCBM volume fit, respectively. Legend colors apply to all sub-graphs.